Chapter 1

Introduction

1.1 History of Vacuum Microelectronics

1.1.1 Overview of vacuum microelectronics

Vacuum tubes have been gradually replaced by solid state electronic devices since the invention of solid state transistors in the late 1940s for the tiny volume, low cost, better reliability, and more power efficient of solid state devices. For the past decades, great improvements on semiconductor manufacturing technology gave a new life to vacuum electronics for the professional micro fabrication process to fabricate tiny vacuum devices, which is now called vacuum microelectronics. "Vacuum state" devices have a great deal of superior advantages as compared with solid-state devices, including fast carrier drift velocity, radiation hardness, and temperature insensitivity. For example, the saturation drift velocity is limited to less than 3×10^{7} cm/s in all semiconductor due to scattering mechanism whereas the saturation drift velocity in vacuum is limited theoretically to 3×10^{10}cm/s and practically to about $6\text{-}9\times10^{8}$cm/s [1]. Moreover, temporarily or permanently radiation effect is negligible in vacuum devices for no medium can be damaged. Additionally, the effect of temperature on performance is reduced in vacuum devices simply for no medium to cause the temperature effect in semiconductor, such as increased lattice scattering or bulk carrier generation and recombination. Table 1.1 shows the comparison between vacuum microelectronic and semiconductor devices. Table 12 shows the evolution of CNTs history.

Recent development in vacuum microelectronics started in 1928, when R. H. Fowler and L. W. Nordheim published the first theory of electron field emission from metals using quantum mechanics [2]. This theory is contrary to thermionic emission, which metals have to be heated so that some of the electrons in metal gain enough

thermal energy to overcome the metal/vacuum barrier; according to the Fowler-Nordheim theory, an applied electric field of approximately 10^3 V/μm is needed for electrons to tunnel through the sufficiently narrow barrier [2]. To reach this high field at reasonable applied voltage, producing the field emitters into protruding objects is essential to take advantage of field enhancement. It was not until 1968 when C. A. Spindt camp up with a fabrication method to create very small dimension metal cones that vacuum microelectronic triodes became possible [3]. From the late 1960s to the year 1990, Ivor Brodie, Henry F. Gray, and C. A. Spindt made many contributions to this field. Also, most of research was focused on the devices similar to the Spindt cathode during the past three decades.

In 1991, a group of research of the French company LETI CHEN reported a microtip display at the fourth International Vacuum Microelectronics Conference [4]. Their display was the first announcement of a practical vacuum microelectronic device. From then on, a great amount of researchers all over the world devoted themselves to this interesting, challenging, and inventive field. Part of the work focused on fabricating very small radius silicon tip by utilizing modern VLSI technology [5-6]. Some of them increased the emission current by coating different metals, such as W, Mo, Ta, Pt etc., even diamond on field emission arrays [7-9]. Different device schemes also have been proposed to enhance the emission current density, stability, and reliability.

1.1.2 Theory Background

Electron field emission is a quantum mechanical tunneling phenomenon of electrons extracted from the conductive solid surface, such as a metal or a semiconductor, where the surface electric field is extremely high. If a sufficient electric field is applied on the emitter surface, electrons will be emitted through the surface potential barrier into vacuum, even under a very low temperature. In contrast, thermionic emission is the hot electron emission under high temperature and low

electric field. Figs. 1.1(a) demonstrates the band diagram of a metal-vacuum system.

Here W_0 is the energy difference between an electron at rest outside the metal and an electron at rest inside the metal, whereas W_f is the energy difference between the Fermi level and the bottom of the conduction band. The work function ϕ is defined as $\phi = W_0 - W_f$. If an external bias is applied, vacuum energy level is reduced and the potential barrier at the surface becomes thinner as shown in Figs. 1.1(b). Then, an electron having energy "W" has a finite probability of passing through the surface barrier. Fowler and Nordheim derive the famous F-N equation (1.1) as follow [2]:

$$J = \frac{aE^2}{\phi t^2(y)} \exp[-b\phi^{\frac{3}{2}} v(y)/E], \qquad (1\text{-}1)$$

where J is the current density (A/cm^2). E is the applied electric field (V/cm), ϕ is the work function (in eV), $a = 1.56\times10^{-6}$, $b = -6.831\times10^{-7}$, $y = 3.79x10^{-4}\times10^{-4}E^{1/2}/\phi$, $t^2(y)$~1.1 and v(y) can be approximated as [1.10]

$$v(y) = \cos(0.5\pi y), \qquad (1\text{-}2)$$

or

$$v(y) = 0.95 - y^2. \qquad (1\text{-}3)$$

Typically, the field emission current I is measured as a function of the applied voltage V. Substituting relationships of $J = I/\alpha$ and $E = \beta V$ into Eq.(1-1), where α is the emitting area and β is the local field enhancement factor at the emitting surface, the following equation can be obtained

$$I = \frac{A\alpha\beta^2 V^2}{\phi t^2(y)} \exp[-bv(y)\frac{\phi^{\frac{3}{2}}}{\beta V}]. \qquad (1\text{-}4)$$

Then taking the log. form of Eq. (1-4) and v(y) ~ 1

$$\log(\frac{I}{V^2}) = \log[1.54\times10^{-6}\frac{\alpha\beta^2}{\phi t^2(y)}] - 2.97\times10^7(\frac{\phi^{3/2}v(y)}{\beta V}), \qquad (1\text{-}5)$$

from Eq. (1-5), the slope of a Fowler-Nordheim (F-N) plot is given by

$$S \equiv slope_{FN} = -2.97 \times 10^{7} (\frac{\phi^{\frac{3}{2}}}{\beta}), \quad (1\text{-}6)$$

The parameter β can be evaluated from the slope S of the measured F-N plot if the work function ϕ was known

$$\beta = -2.97 \times 10^{7} (\frac{\phi^{\frac{3}{2}}}{S}) \ \ (\text{cm}^{-1}), \quad (1\text{-}7)$$

The emission area α can be subsequently extracted from a rearrangement of Eq. (1-5)

$$\alpha = (\frac{I}{V^{2}}) \frac{\phi}{1.4 \times 10^{-6} \beta^{2}} \exp(\frac{-9.89}{\sqrt{\phi}}) \exp(\frac{6.53 \times 10^{7} \phi^{\frac{3}{2}}}{\beta V}) \ \ (\text{cm}^{2}). \quad (1\text{-}8)$$

For example, the electric field at the surface of a spherical emitter of radius r concentric with a spherical anode (or gate) of radius r + d can be represented analytically by

$$E = \frac{V}{r} (\frac{r+d}{d}), \quad (1\text{-}9)$$

Though a realistic electric field in the emitter tip is more complicated than above equation, we can multiple Eq. (1-9) by a geometric factor $\beta`$ to approximate the real condition.

$$E_{tip} \equiv \text{function of (r,d)} = \beta` \frac{V}{r} (\frac{r+d}{d}), \quad (1\text{-}10)$$

where r is the tip radius of emitter tip, d is the emitter-anode(gate) distance and $\beta`$ is a geometric correction factor [11].

For a very sharp conical tip emitter, where d >> r, E_{tip} approaches to $\beta`$(V/r). And for r>>d, $E_{tip}$ approaches to $\beta`$(V/d) which is the solution for a parallel-plate capacitor and for a diode operation in a small anode-to-cathode spacing.

As the gated FEA with very sharp tip radius, Eq. (1-10) can be approximated as:

$$E_{tip} = \beta`(V/r). \quad (1\text{-}11)$$

Combining E = βV and Eq. (1-11), we can obtain the relationship:

$$E_{tip} = \beta V = \beta`(V/r), \text{ and } \beta` = \beta r. \tag{1-12}$$

The tip radius r is usually in the range from a few nm to 50 nm, corresponding to the parameter $\beta`$ ranging from 10^{-1} to 10^{-2}.

Besides, transconductance g_m of a field emission device is defined as the change in anode current due to a change in gate voltage [1].

$$g_m = \frac{\partial I_C}{\partial V_g}|_{Vc}, \tag{1-13}$$

Transconductance of a FED is a Figsure of merit that gives as an indication of the amount of current charge that can be accomplish by a given change in grid voltage. The transconductance can be increase by using multiple tips or by decreasing the gate-to-cathode spacing for a given anode-to-cathode spacing.

According to the above mention equations (especially Eq.1-5), the following approaches may therefore be taken to reduce the operating voltage of the field emission devices:

1) Find techniques to reproducibly sharpen the tips to the atomic level (increase β).
2) Lower the work function of the tip (ϕ).
3) Narrow the cone angle (increase β).
4) Reduce the gate-opening diameter (increase β).

1.2 Applications of Vacuum Microelectronic Devices

Due to the superior properties of vacuum microelectronic devices, potential applications include high brightness flat-panel display [12-16], high efficiency microwave amplifier and generator [17-19], ultra-fast computer, intense electron/ion sources [20-21], scanning electron microscopy, electron beam lithography, micro-sensor [22-23], temperature insensitive electronics, and radiation hardness analog and digital

circuits

1.2.1 Vacuum Microelectronic Devices for Electronic Circuits

Either vacuum or solid-state devices can generate power at frequency in the GHz range. Solid-state devices, such as impact avalanche transit time (IMPATT) diodes, Si bipolar transistors, and GaAs FETs [24], are typically used in the lower power (up to 10 W) and frequency (up to 10 GHz) range. Vacuum devices still remain the only technology available for high power and high frequency applications. These devices include traditional multi-terminal vacuum tubes, like triodes, pentodes, and beam power tubes, and distributed-interaction devices, such as traveling wave tubes (TWTs), klystrons, backward-wave oscillators (BWOs).

The performance of FEAs in conventionally modulated power tubes, like TWT, is determined primarily by their emission current and current density capability. On the other hand, application of FEAs in the microwave tubes in which modulation of the beam is accomplished via modulation of the emission current at source, such as capacitance and transconductance. Successful operation of a gated FEA in a 10 GHz TWT amplifier with conventional modulation of electron beam has been demonstrated by NEC Corporation of Japan [25]. The amplifier employed a modified Spindt-type Mo cathode with circular emission area of 840 μm in diameter. The modified cathode structure incorporated a resistive poly-Si layer as a current limiting element. The emission current from the cathode was 58.6 mA. The prototype TWT could operate at 10.5 GHz with the output power of 27.5 W and the gain of 19.5 dB. The bandwidth of the tube was greater than 3 GHz. The prototype was operated for 250 h.

1.2.2 Field Emission Displays

Among wide range applications of the vacuum microelectronics, the first commercial product could be the field emission flat-panel display. The field emission fluorescent display is basically a thin cathode ray tube (CRT) in Figs. 1.2(a), which was

first proposed by SRI International and later demonstrated by LETI [4].

Various kinds of flat-panel displays are developed for the better characteristics of small volume, light weight, and low power consumption, as shown in [35] [36][37] :

(a) Vacuum fluorescent display (VFD) as shown in Figs. 1.2(b).

(b) Plasma display panel (PDP) as shown in Figs. 1.2(c)

(c) Field Emission display (FED) : as shown in Figs. 1.2(d)

LCDs have become the most popular flat panel displays, however, LCDs have some drawbacks, such as poor viewing angle, temperature sensitivity and low brightness. As a result, some opportunities still exist and waiting for the solutions from other flat panel displays such as FED.

FED features all the pros of the CRTs in image quality and is flat and small volume. The schematic comparisons are revealed in Figs. 1.2 (a)(d)[35][36][37]. The operation of CRTs involves deflection of the beam in such a way that the electron spot scans the screen line-by-line. In FEDs, multiple electron beams are generated from the field emission cathode and no scanning of beams is required. The cathode is a part of the panel substrate consists of an X-Y electrically addressable matrix of field emission arrays (FEAs). Each FEA is located at the intersection of a row and a column conductor, with the row conductor serving as the gate electrode and the column conductor as the emitter base. The locations where the rows and columns intersect define a pixel. The pixel area and number of tips are determined by the desired resolution and luminance of the display. Typically, each pixel contains an FEA of 4-5000 tips. The emission current required for a pixel varies from 0.1 to 10 μA, depending on the factors such as the luminance of the display, phosphor efficiency and the anode voltage.

Compared to the active matrix LCDs, FEDs generate three times the brightness with wilder viewing angle at the same power level. Full color FEDs have been developed by various research groups from different aspects such as PixTech, Futaba,

Fujitsu, Samsung, are presently engaged in commercially exploiting FED.

1.3 Recent Developments of Field Emission Devices for Field Emission Displays

FED is one of the most promising emissive type flat-panel display, which can overcome the drawbacks of TFT-LCD. However, some difficult technological subjects should be considered such as microfabrication of cathodes, assembly technology with accuracy of micrometer level, packaging of vacuum panel with thin-glass substrates, vacuum technology to keep stable field emission in small space of flat panels, selection of suit-able materials to keep a high vacuum condition in panels and high efficiency phosphor materials. The research objective of this thesis is to produce novel cathode structure and synthesis of novel emitter materials for FED operations. The experimental background is introduced in the following sections.

1.3.1 Cathode Structures and Materials for Field Emission Displays

A. Spindt-type field emitters

A spindt type field emission triode [26] was invented by Spindt of SRI and improved for the electron source of high-speed switching devices or microwave devices [27]. Meyer of LETI presented the capability of using Spindt-type emitters for a display in 1970s [28] and stabilized the field emission from Spindt-type emitters by introducing a resistive layer as the feedback resistance. This proposal triggered the development of field emitters as an electron source of displays by researchers and electronics makers in 1990. The merits of the Spindt type field emitters are summarized as following: (1) High emission current efficiency, more than 98% anode current to cathode current can be achieved for the symmetric structure of Spindt tip and the gate hole, the lateral electric field to the metal tip can be cancelled out. (2) The fabrication is self-aligned, easy process; uniform field emission arrays can be fabricated easily. Some research groups have successfully fabricated commercial FED products based on Spindt type

field emitters such as Futaba, Sony/Candesent, Futaba and Pixtech.[29], the products of above mentioned companies are shown [38] [39][40][41].

However, there are some existing drawbacks of Spindt type field emitters when fabricating Spindt type FED such as (1) High gate driving voltage required; for a Spindt type field emission triode with 4 μm gate aperture, the driving voltage is typically more than 60 V, which results in the high cost of the driving circuits. To reduce the gate driving voltage, frontier lithography technologies such as E beam lithography must be applied to reduce the gate aperture to the sub-micron level. (2) The emission property degrades for the chemically instable of the metal tips. (3) Huge, expensive high vacuum deposition system required during fabricating large area Spindt type FED.

B. Si tip field emitters

An alternative approach to fabricate tip type field emitters is to fabricate the Si tip field emitters based on the semiconductor fabricating process. Figs. 1.4 [37] depict the SEM micrographs of Si tips array and Si tip field emission triodes array formed by chemical mechanical polishing (CMP) [30] Symmetric device structure and similar advantages with Spindt type field emitters can be obtained, However, high temperature oxidation sharpening process [5] prohibits Si tip from large area fabrication.

C. Carbon and Nano-sized Emitters

Carbon nanotubes have attracted a great deal of interest owing to their advantageous properties, such as high aspect ratios, small tip radius of curvature, high Young's modulus, capability for the storage of a large amount of hydrogen, and structural diversities that make it possible for band gap engineering. These useful properties of carbon nanotubes (CNTs) make themselves good candidates for various applications, for instance, wires for nanosized electronic devices, super strong cables, AFM tips, charge-storage devices in battery, and field emission display.

According to Fowler-Nodiem theory, the electric field at the apex of a

needle-shaped tip is enhanced by a factor $\beta = h/r$, where h is the height of the tip and r is the radius of curvature of the tip apex. The carbon nanotube is a stable form of carbon and can be synthesized by several techniques. They are typically made as threads about 10-100 nm in diameter with a high aspect ratio (>1000). These geometric properties, coupled with their high mechanical strength and chemical stability, make carbon nanotubes attractive as electron field emitters. Several groups have recently reported good electron field emission from nanotubes [31-33].

In 1999, Samsung pronounced a 4.5-inch carbon nanotube based field emission display. They mixed a conglomeration of single-walled CNTs into a paste with a nitrocellulose binder and squeezed the concoction through a 20-μm mesh onto a series of metal strips mounted on a glass plate. As the CNTs emerged from the mesh, they were forced into a vertical position. The metal strips with the CNTs sticking out of them served as the back of the display. The front of the display was a glass plate containing red, green, and blue phosphors and strips of a transparent indium-tin-oxide anode running from side to side. The glass plates were separated by spacers with the thickness of 200 μm. Once assembled, the edges were sealed and air was pumped out of the display.

Samsung's field emission display in Figs. 1.5 could be the precursor of a new generation of more energy efficient, high performance flat panel displays for portable computers [34]. The CNTs appear to be durable enough to provide the 10000-h lifetime considered being a minimum for an electronic product. The panel consumes just half the power of an LCD to generate an equivalent level of screen brightness. They could also be cheaper than LCDs or other types of field emission displays being developed. Until now, at last five major Japanese electronic manufactures are working on this technology.

1.4 Motivation

Fabricating field emission cathodes with low operation voltage, high emission current, excellent stability and good reliability is crucial to commercialize the field emission devices. According to the F-N equation, to achieve the high emission currents at low applied voltages, the work function ϕ of the cathode material must be as low as possible and the field-enhancement factor β and emission area α should be as large as possible.

To obtain a large β, the conventional method is to produce sharp tips, which required special techniques or complicated fabrication process, such as large oblique-angle thermal evaporation or sputtering to produce sharp metal cones, high temperature oxidation to sharpen silicon tips, or anisotropic etching of silicon using KOH to fabricate sharp tip molds. However sharp tips field emission devices have poor emission site densities, it needs complicated process to produce high emission current site densities.

In recent years carbon nanotubes (CNTs) have drawn considerable attraction, because CNTs were synthesized as the field emitters for the nano-sized feature, which can provide large aspect ratio to increase the field enhancement factor β. The high density of the nanotubes also provides the large emission site density (increasing the emission area α). The field emission properties of carbon nanotubes (CNTs) were enhanced by argon & oxygen ions Plasma-Post-Treatment (PPT). PPT led to an enhancement in the emission properties of CNTs which showed a decrease in turn-on field and an increase in total emission current after the treatment. The PPT permanently straightened as-grown curly CNTs, and, as a result, the local electric field was increased, due to the increased aspect ratio and reduced mutual shield effect. In addition, increased defects, produced by the PPT are likely to make their effective surfaces more active, thus emitting more electrons. !

1.5 Thesis Organization

The overview of vacuum microelectronics and basic principles of field emission theory are described in chapter 1.

Chapter 2 introduced the characteristics of the CNTs, the method of carbon nanotubes synthesis and the mechanism of CNTs growth.

Experimental procedures and field emission devices were fabricated in chapter 3. Combining semiconductor thin film technology and selective-area growth of CNTs, the field emission CNTs diode can be easily obtained by easy lithographic tool. Thermal CVD method has been successful to produce the CNTs in large quantity, and also to obtain the vertically aligned CNTs.

Chapter 4 revealed the synthesis of the CNTs for effects of different growth parameters and the improved field emission characteristics of carbon nanotubes by argon (Ar) & oxygen (O_2) Plasma-Post-Treatment (PPT). Then, the Plasma-Post-Treatment (PPT) process is introduced to improve the emission current density and the turn on voltage of CNTs. We treated the Thermal CVD CNTs with different PPT conditions, including different generation RF power (ICP & Bias power), plasma flow rates and plasma etching time. In addition to, the CNTs triode structures with an extraction gate were proposed to achieve the low voltage modulation. CNTs triodes device were fabricated by the semiconductor fabrication process, which utilized the selective growth of CNTs and controlled density of CNTs to reduce the turn-on gate voltage. The gate-to-emitter gap can be reduced to 1 μm. The device can be turned on below the anode voltage of 1000 V.

Finally, the conclusions and recommendations for future researches are provided in chapters 5.

Chapter 2

Overview

2.1 Paper Study

Carbon nanotubes (CNTs) grown on the cathode of an arc discharge were first observed by Iijima in 1991 [60]. The discovery of multi-walled carbon nanotubes (MWNTs) has attracted considerable interests because of their own unique physical properties and potential for the variety of applications [61-63]. Due to its geometrical properties, such as high aspect ratios, small tip radii of curvature, high electrical conductivity, high mechanical strength, chemical stability, super thermal conductivity, and the excellent field emission characteristics. CNTs can be produced by arc discharge [64-65], laser ablation [66], thermal chemical vapor deposition [67-68], and microwave plasma-enhanced chemical vapor deposition [69]. However, the diameter distribution and the density of CNTs still cannot be controlled effectively. The screening effect of the dense arrangement CNTs by electric field has been reported [70-72]. The density of CNTs at the film surface determines the emission sites density. If the CNTs are too closely packed, the electric field will be screened out. Groning *et al.* reported the field enhancement factor β of the tips decreases rapidly when the inner tip spacing is smaller than twice the length of the tips. They also found that the maximum current density was obtained when the spacing between the tips is about two times of their relative heights by simulations. For larger spacing, the current density decreases due to the decreasing density of the tips, with a nearly constant emission current per tip as the field enhancement factor remains constant. For smaller spacing the current density decreases rapidly due to the decreasing β factor and this effect cannot be compensated for by the quadratic increasing density of the emitting tips. This shows that when the spacing

between the emitting structures on a surface becomes comparable to its length, problems of shielding do occur and will limit the emission current density.

Because CNTs exhibit extremely high electron emission current at low operating voltage due to high aspect ratio, CNTs have been regarded as a strong candidate for field emission display. The density of CNTs plays a crucial role for the field emission properties. For high density CNTs film, screening effect reduced the field enhancement and thus the reduced emitted current. Therefore it is important to control the density of CNTs for field emission application.

Recently, plasma post treatment are use to etch the surface of CNTs and change the density of CNTs film. Plasma post treatment has several effects as follows. First, changes the structure of carbon nanotubes on their walls and tips. Second, purifies the carbon nanotubes by eliminating amorphous carbon. Third, changing the density of CNTs and causing defects on CNTs film. Therefore, to optimize the density of CNTs and to obtain better field emission properties, proper plasma post treatments on CNTs are needed. Several plasma post treatment methods [79-83] including H_2, Ar and O_2 plasma were reported to improve the field emission properties of CNTs, but these methods do not improve the field emission properties very well.

2.2 Structure and Characteristics of Carbon Nanotubes

The discovery of nanotubes happened in 1991 when Sumio Iijima of NEC Corporation found these tiny needles, consisting of concentric graphite tubes, on the electrodes used to prepare fullerenes [40]. Nanotubes can be divided into two categories. The first is called multiwall carbon nanotubes (MWNTs). MWNTs are close to hollow graphite fibers [41][43], except that they have a much higher degree of structural perfection. They are made of sheets of carbon atoms with a cylindrical shape and generally consist of co-axially arranged 2 to 20 cylinders, as shown in Fig. 2.1(b). This

is attributed to a combination of tubule curvature and van der Waals force interactions between successive graphite layers. The second type of the nanotube is made up of just a single layer of carbon atoms. These nanotubes are called the single-walled nanotubes (SWNTs) and possess good uniformity in diameter about 1.2 nm, as shown in Fig. 2.1(a). They are close to fullerenes in size and have a single-layer cylinder extending from end to end [42][43].

Carbon nanotubes consist of concentric hexagon-rich cylinders, made up of sp^2 hybridized carbon, as in graphite, and terminated by end-caps arising from the presence of 12 pentagons (six per end). It is possible to construct a cylinder by rolling up a hexagonal graphene sheet in different ways. Two of these are "non-helical" in the sense that the graphite lattices at the top and bottom of the tube are parallel. These arrangements are named "armchair" and "zig-zag" in Figs. 2.2(a)-(c).

A carbon nanotube is based on a two-dimensional graphite sheet in Figs. 2.4(a)-(c). (a) The chiral vector is defined on the hexagonal lattice as $C_h = n\hat{a}_1 + m\hat{a}_2$, where $\hat{a}_1$ and $\hat{a}_2$ are unit vectors, and n and m are integers. The chiral angle q is measured relative to the direction defined by $\hat{a}_1$. This diagram has been constructed for $(n, m) = (4, 2)$, and the unit cell of this nanotube is bounded by OAB'B. To form the nanotube, imagine that this cell is rolled up so that O meets A and B meets B', and the two ends are capped with half of a fullerene molecule. Different types of carbon nanotubes have different values of n and m. (b) Zigzag nanotubes correspond to $(n, 0)$ or $(0, m)$ and have a chiral angle of 0°, armchair nanotubes have (n, n) and a chiral angle of 30°, while chiral nanotubes have general (n, m) values and a chiral angle of between 0° and 30°. According the theory, nanotubes can either be metallic (green circles) or semiconductor (blue circles) [49][52]. (c) Schematic diagram showing how a hexagonal sheet of graphite is 'rolled' to form a carbon nanotube.

2.3 The Method of Carbon Nanotubes Synthesis

2.3.1 Arc-discharge methods [51]

Iijima [40] first observed nanotubes synthesized from the electric-arc discharge technique. Shown schematically in Fig. 2.5 (a), the arc discharge technique generally involves the use of two high-purity graphite rods as the anode and cathode. The rods are brought together under a helium atmosphere and a voltage is applied until a stable arc is achieved. The exact process variables depend on the size of the graphite rods. As the anode is consumed, a constant gap between the anode and cathode is maintained by adjusting the position of the anode. The material then deposits on the cathode to form a build-up consisting of an outside shell of fused material and a softer fibrous core containing nanotubes and other carbon particles. To achieve single walled nanotubes, the electrodes are doped with a small amount of metallic catalyst particles.

2.3.2 Laser vaporization [41]

Laser ablation was first used for the initial synthesis of fullerenes. Over the years, the technique has been improved to allow the production of single-walled nanotubes. In this technique, a laser is used to vaporize a graphite target held in a controlled atmosphere oven at temperatures near 1200℃. The general set-up for laser ablation is shown in Fig. 2.5 (b). To produce single-walled nanotubes, the graphite target was doped with cobalt and nickel catalyst. The condensed material is then collected on a water-cooled target. Both the arc-discharge and the laser-ablation techniques are limited in the volume of sample they can produce in relation to the size of the carbon source (the anode in arc-discharge and the target in laser ablation). In addition, subsequent purification steps are necessary to separate the tubes from undesirable by-products.

2.3.3 Chemical vapor deposition

The arc-discharge and laser ablation techniques generate thin CNTs, but they include significant amounts of fibers, soot, and other carbon synproducts. These processes have very limited ability to control the growth of these unwanted deposits. Since separation of CNTs is difficult and the yield is low, they are very expensive. However, the catalytic CVD technique, which employs the catalytic decomposition of short-chain hydrocarbons, can produce relatively large amounts of CNTs under mild conditions. Moreover, this process makes it possible to control the size and growth density of CNTs by dispersing the catalyst particles on supports and adjusting the reaction parameters at relatively lower temperatures in comparison with the former processes [57].

These limitations have motivated the development of gas-phase techniques, such as Thermal Chemical Vapor Deposition (Thermal CVD) and Microwave Plasma Enhanced Chemical Vapor Deposition (MPECVD) in Figs. 2.5 (c) and (d), where nanotubes are formed by the decomposition of a carbon-containing gas. The gas-phase techniques are amenable to continuous processes since the carbon source is continually replaced by flowing gas. In addition, the final purity of the as-produced nanotubes can be quite high, minimizing subsequent purification steps [49][50][56].

2.4 The Mechanism of Carbon Nanotubes Growth

2.4.1 CNTs growth mechanism

A typical growth condition may involve the following step in Fig. 2.6 (a) hydrocarbon dissociate & deposit carbon on surface, (b) carbon diffuses through solid metal, and (c) carbon precipitates as curved graphitic layers [78].

2.4.2 Influence of the metal-support interaction for tip growth mode and base growth (root growth) mode

Based on the position of metal particle on the tube, there were two kinds of growth mode : one is called “base-growth” in Fig. 2.7(a) and the other is called “tip-growth” in Fig. 2.7(b). The “base-growth” mode meant that the tube grew upward from metal particles, which attached to the substrate. If the metal particle detached and moved to the head of the growing tubes, it was the “tip-growth” mode [53][54]. (c) 2.8 Combined tip growth and base growth [59].

Chapter 3

Experimental Procedures

3.1 Fabrication Procedure of Carbon Nanotubes for Diode Devices

Experimental procedures flow charts such as Fig. 3.1 The schematic fabrication flow is shown in Fig. 3.2 and Fig. 3.3 and the detailed procedures are illustrated as follow.

3.1.1 Sample preparation

(a) Standard RCA initial cleaning procedure is applied to (100) oriented, phosphorous doped 4 inches silicon wafer with a resistivity 4~7Ω-cm, as shown in Fig. 3.2(a).

(b) A 2000Å thickness positive photoresist was spun on and patterned then was exposed (Mask2) to form the different hole size such as 1000µm x 1000µm, 100µm x 100µm and 10µm x 10µm, as shown in Fig. 3.2(b)(c)(d).

3.1.2 Buffer layer and metal catalyst deposition by Electron Beam Evaporation (E-GUN)

(a) A thin buffer layer of about 500Å thickness was deposited by E-GUN and RF magnetron sputtering, such as Ti, as shown in Fig. 3.2(e).

(b) A thin Fe-Ni (1:1) alloy layer of about 50Å thickness was deposited by electron beam evaporation, as shown in Fig. 3.2(f).

(c) After the photoresistance was removed by the lift-off method, the Fe-Ni layer was formed in the self-aligned emitter area, as shown in Fig. 3.2(g).

3.1.3 CNT growth by Thermal Chemical Vapor Deposition (Thermal CVD)

(a) Carbon nanotubes were grown selectively on the Fe-Ni layers by thermal chemical vapor deposition (Thermal CVD). The reaction gases were CH_4, C_2H_4, N_2 and H_2, and flow rates were 200 sccm, 10~138 sccm, 500 sccm and 500sccm, respectively. The chamber temperature were at 500~700°C and the deposition time was 5~15 minutes, as shown in Fig. 3.2(h) and Fig. 3.5 CNT growth procedure by Thermal CVD process.

(b) Experimental parameters in Tables 3-1~3-2

Table 3-1 : Conditions of different pretreatment times and catalyst layer thickness.

Table 3-2 : Conditions of C_2H_4 flow rate for CNT growth lengths(700˚C).

3.1.4 Controlled Density of CNTs by HDP Post-Treatment

(a) Experimental parameters as Table 3-3 list.

(1) Table 3-3 : Conditions of Ar or/and O_2 mixture gas HDPPT for diode.

(b) The pressure of ICP system was 10 mTorr and the high density plasma argon (Ar) and the oxygen (O_2) flow rate were 5~40 sccm. The density of carbon nanotubes were modified by ICP RF such as etchant, power and etching time. The schematic fabrication flow is shown in Figs. 3.2(a)-(c).

(c) Plasma can break the chemical bond and generate free radical by dissociation collision. Free radical can enhance physical and chemical reaction in CVD processes.

3.2 Fabrication of Carbon Nanotubes for Field Emission Triode Devices

3.2.1 Sample preparation

(a) Standard RCA initial cleaning procedure is applied to Si (100) oriented, phosphorous doped 4 inches silicon wafer with a resistivity 4~7Ω-cm, as shown in Fig. 3.3(a).

(b) A 1μm thickness wet thermal dioxide growth on a n-type Si (100) in a H_2 (24sccm) and O_2 (24sccm) steam ambient 1050°C for 3 hours, as shown in Fig. 3.3(b).

(c) Poly gate electrode formation by LPCVD : A 2000Å thickness poly Si was then deposition as the gate electrode by low pressure chemical vapor deposition (LPCVD) in SiH_4 (40sccm) ambient 620°C pressure 120mtorr for 25 minutes to grow 2000Å poly-silicon, as shown in Fig. 3.3(c).

(d) Doped with phosphorous using solid diffusion source $POCl_3$ (24sccm), O_2 (28sccm) and N_2 (40sccm) at 950°C for 30 minutes, as shown in Fig. 3.3(d).

(e) HF dip native oxide from procedure (d).

(f) A 2000Å thickness positive photoresist (FH-6400) on 2000r.p.m for 5 seconds at low speed and 3700r.p.m for 25 seconds at high speed was spun on to remove the poly and oxide of wafer back side. Etching the poly and oxide

of wafer back side by poly and BOE solution, then lift-off photoresist, as shown in Figs. 3.3(e)(f).

(g) A 2000Å thickness positive photoresist (FH-6400) on 2000r.p.m for 5 seconds at low speed and 3700r.p.m for 25 seconds at high speed was spun on and patterned then was exposed (Mask1) at 40 seconds to form the poly gate of slot type.

(h) Etching poly gate by poly solution, and lift-off photoresist.

(i) A 8000Å thickness positive photoresist (AZ-4620) on 2000r.p.m for 20 seconds at low speed and 4000r.p.m for 30 seconds at high speed was spun on and patterned then was exposed (Mask2) to form the different hole size such as 1000μm x 1000μm, 100μm x 100μm and 10μm x 10μm, as shown in Fig. 3.3(g).

(i) The poly Si layer was etched by the ICP-RIE with Cl_2 (40sccm), SF_6 (10sccm) and O_2 (5sccm) mixture gas for 1minute, and the SiO_2 layer was continuously etched by the ICP-RIE using CHF_3 (40sccm) and Ar (40sccm) mixture gas for 8.5 minutes and 40 seconds, as shown in Fig. 3.3(h).

(j) The Si layer was etched about 4μm by the ICP-RIE with SF_6 (40sccm) and O_2 (4sccm) mixture at 3 minutes, as shown in Fig. 3.3(i).

(j) The patterned sample was continuously wet etching in dioxide anti-tropic etching solution by BOE at 5 minutes, and under cut of silicon dioxide was therefore as gate-to-emitter gap to avoid the short circuit problem, as shown in Fig. 3.3 (j)(k)(l).

3.2.2 Buffer layer and metal catalyst deposition

(a) A thin buffer layer of about 500Å thickness was deposited by E-GUN and RF magnetron sputtering, such as Ti, as shown in Fig. 3.3(m).

(b) A thin Fe-Ni (1:1) alloy layer of about 50Å thickness was deposited by electron beam evaporation, as shown in Fig. 3.3(n).

(c) After the photoresist was removed by the lift-off method, the Fe-Ni layer was formed in the self-aligned emitter area, as shown in Fig. 3.3(o).

3.2.3 CNT growth by Thermal Chemical Vapor Deposition (Thermal CVD)

(a) Carbon nanotubes were grown selectively on the Fe-Ni layers by thermal chemical vapor deposition (Thermal CVD). The reaction gases were CH_4, C_2H_4, N_2 and H_2, and flow rates were 200 sccm, 10~138 sccm, 500 sccm and 500sccm respectively. The ambient temperature was at 700°C and the

deposition time was 5~15 minutes, as shown in Fig. 3.3(p).

(b) Experimental Parameters as Table 3-2.

(1) Table 3-2 : Conditions of C_2H_4 flow rate for CNT growth lengths(700°C).

3.2.4 Controlled Density of CNTs by HDP Post-Treatment

(a) Experimental parameters as Table 3-3.

Table 3-3 : Conditions of Ar or/and O_2 mixture gas HDPPT

(b) The pressure of ICP system was 10 mTorr and the high density plasma argon (Ar) 20sccm and the oxygen (O_2) 10 sccm . The density of carbon nanotubes were modified by ICP RF such as etchant, power and etching time. The schematic fabrication flow is shown in Figs. 3.4(a)-(c)

(c) Plasma can break the chemical bond and generate free radical by dissociation collision. Free radical can enhance physical and chemical reaction in CVD processes.

3.3 Measurement System

3.3.1 Field Emission Measurement (Fig. 3.5 (a) (b))

Field emission properties of the deposited CNTs were characterized in a high-vacuum environment with a base pressure of 1.0×10^{-7} Torr. The phosphor coated indium-tin-oxide (ITO) glassr was positioned 100 μm above the sample surface as an anode. The emission current densities of the CNTs were measured as a function of applied electric field, using Keithley 237 high voltage source measure units and an IEEE 488 interface controlled by a personal computer. The cathode luminescence could be obtained from the phosphor plate.

3.3.2 Scanning Electron Microscopy (SEM) was Employed for the Analysis of the Morphology and Density CNTs

Scanning electron microscopy (SEM, Hitachi S-4700) were utilized to observe the lengths, diameters, density and the morphologies of the CNTs arrays before and after treatment.

3.3.3 The CNTs were Characterized by Raman Spectroscopy

When the silicon or the carbon have netted structure of covalent, the atom shows its Ramon's spectrum in the highest vibration of balanced location promptly, and offer the information between the crystallization and atom band.

3.3.4 High-Resolution Transmission Electron Microscopy (TEM) was Adopted for the Microstructure Analysis of CNTs

High resolution transmission electron microscope (HRTEM, JEOL-JEM3011) at 300 kV were utilized to discover the microstructural analysis of the CNTs.

3.3.5 An Energy Dispersive X-Ray (EDX) Analyzer was Used to Investigate the Composition of the Fe-Ni Surface

An energy dispersive X-ray (EDX) analyzer was used to investigate the composition if Fe-Ni surface before and after plasma post treatment

Chapter 4

Results and Discussions

Vertically alignment of CNTs on the substrate is crucial for the practical application as field emitters on substrates or glass [59]. The growth results of the carbon nanotubes were discussed. Different morphology of CNTs compare with the varying growth of parameters. The synthesis of CNTs from different transition metal of the catalyst also has been investigated. The better field emission characteristics of the CNTs could be obtained from suitable growth parameters and different morphology.

In the experimental, the high density of carbon nanotubes (CNTs) were deposited by thermal chemical vapor deposition (Thermal CVD), which results in screening effect [60] in the electric field. To obtain better field emission properties, the density of CNTs should be optimized by parameters control. In this chapter, a novel process using high-density plasma post-treatment (HDPPT) and modify the density of CNTs was proposed. Various arrangements of CNTs were utilized by different plasma generating power density, plasma gas flow rate and plasma etching time.

Especially, triode type CNT field emitter have some advantages such as field emission at a lower electric field, uniformity and stability of the field emission, easy adjustment, and high quality screen, compared with diode type CNT emitters in display application of CNTs.

4.1 The Chrematistics of Carbon Nanotubes and Field Emission array by Thermal CVD

4.1.1 Thickness Effects of Catalyst Layer

Figure 4.1 shows that the SEM images of Fe-Ni films with varying thickness after pre-treatment. The Fe-Ni film was nucleated into small nanoparticles due to the surface tension, compressive stress and thermal expansion coefficients of Ti and Fe-Ni mismatch [64]. Figs. 4.1(a)-(d) shows AFM images of the catalytic metal surface roughness. The surface roughness distribution can enhanced carbon feedstock and diffusion which promote the growth of CNTs. It is obvious that the size of nanoparticles depend on the thickness of the Fe-Ni film. Fig. 4.1(e) shows that the average nanoparticles size of proportion with the Fe-Ni layer thickness. The nanoparticle diameter was larger than the catalyst thickness. Nanoparticle and growth of CNTs were difficultly to form from the thick catalyst films as shown as Fig. 4.1(f). The diameter, length, and density of the CNTs were affected by the thickness of catalyst layer. Fig. 4.1(f) shows the diameter of the CNTs about 1.5~2 times with the catalytic metal thickness.

The non-uniform fragmentation of the catalyst particles was attributed from thick catalyst layers during pre-treatment process. Fe-Ni nanoparticle size and CNT diameters was determined by Fe-Ni film thickness. Clearly, the grown nanotubes with smaller diameter can be known at a faster rate in their height between the larger diameter tubes. Presumably, the larger nano-particles derived from thicker catalyst layer had a smaller surface-to-volume ratio (or constant mass deposition rate), which therefore led to a longer reaction time to achieve the same growth condition [66].

4.1.2 Effects of Pre-Treatment and Deposition Temperatures

CNTs have been grown on Fe, Ni or Fe-Ni alloy catalysts at 500°C~700°C by a thermal CVD using ethylene(C_2H_4) as a carbon source, as shown in Fig. 4.2. Moreover, these Fe-Ni catalysts were pre-treated with hydrogen at a low temperature 500°C, catalytic sites on the surface was covered an amorphous carbon layer, as shown in Fig. 4.2(a).

In order to prevent forming amorphous carbon at low temperature, a low concentration of methane (CH_4) was employed to react with catalyst on the pre-treatment process. The CH_4 free-energy (energy-band) is higher than C_2H_4 because of CH_4 decomposed less carbon species than C_2H_4. It is suspected that excess of carbon was deposited on catalyst surface due to a relatively high concentration of ethylene used C_2H_4, thus the catalyst was poisoned and covered by active sites on the surface. Moreover, abundant carbon atoms were deposited on catalyst surface and forming an amorphous carbon layer, catalyst was passivited by blocking the active site [62].

The amount of carbon source was traced by pre-treat the catalyst, carbon atoms were deposited by catalytic decomposition of hydrocarbon sources could gradually diffuse into Fe-Ni catalysts surface and forming Fe-Ni-C alloy. According to Tammann's rule, the Tammann temperature is roughly equal to 0.33 $T_m{}^o$ K, where T_m is the melting point of metal. The Fe-Ni-C trinary alloy must have a lower Tammann temperature than Fe-Ni catalysts due to the low melting point of Fe-Ni-C system. The lower Tammnann temperature allows carbon to diffuse faster in Fe-Ni-C catalysts than in Fe-Ni catalysts. Therefore, the pre-treatment of Fe-Ni catalysts by CH_4 could favor at low temperature growth of carbon nanotubes which enhances the carbon to diffuse inside Fe-Ni-C particles, as shown in Fig. 4.2(b). Fe-Ni-C alloy catalysts were found to

be more suitable for the growth of CNTs at 500℃ than pure Fe, Ni or Fe-Ni catalysts. Difference of growth characteristics seen among three metals is presumably originated from the differences in solubility of carbon in those catalytic metals. The Fe-Ni-C alloys have the highest solubility of carbon. In the experimental, the growth rate of CNTs was improved significantly by pre-treating the catalyst with a low concentration of carbon source (e.g. methane CH_4) forming Fe-Ni-C alloy during the temperature-rising step before growth [61]. Fig. 4.2(a)-(b) show the CNTs morphology of addition CH_4 before growth at 700℃

In the processing gases, the addition of N_2 was not only enhanced the nucleation of the CNTs but also promoted the formation of bamboo-like CNTs structures [74]. The N_2 gases which can keep the active of catalytic metals for the nucleation of CNTs. It is also conjectured that the N_2 gases directly suppress the decomposition of C_2H_4 into amorphous carbon, as shown in Figs. 4.3(b). During the growth as shown as Figs. 4.3(a), the catalytic metal was passivated to end the growth by amorphous carbon. The existence of N_2 at the initiation of growth maintains many Fe-Ni particles being active as nucleation sites, and consequently, the high-density nucleation of CNTs promotes their vertical alignment [62].

4.1.3 Effects of the C_2H_4 for CNT Lengths

Figure 4.4 shows that well-aligned nanotubes linearly grown from 5% (10sccm) to 16% (80scm) for C_2H_4 concentration, because of the carbon species uniformly to diffuse onto catalyst for syntheses process. The growth of nanotubes with linear condition at a rate of 0.36um/(min。 10sccm) during 700℃. However, C_2H_4 concentrations above 20% (100sccm), the nanotubes length was trended saturation. The reason may been the catalyst have deactivated result in CNTs stop grown or it became more difficult for the reactive carbon species to reach the catalyst particle at the root of the nanotube and continue the growth process through a presumed diffusion and precipitation process.[66]. We postulated that the decrease of the growth rate occurred as a result of the Fe-Ni particle becoming fully enclosed at the nanotube ends. It is notice that nanotubes deposited for a period of time (e.g., less than 20 min) do not contain Fe-Ni particles within their shells at the bottom ends with TEM observation, as shown in Fig. 4.5. Consequently, it became more difficult for the reactive carbon species to reach the catalyst particles at the root of the nanotubes and continue the growth process through a presumed diffusion and precipitation process [67].

It will be different for the diffusion flux with the particle size, which is proportional to its surface area of the particle. Therefore the smaller particles, having higher surface-to-volume ratios, will be saturated in a shorter time leading to an earlier initiation of the growth [63].

4.2 Effects of Field Emission on the Characteristics of Carbon Nanotubes Diodes High-Density-Plasma Post Treatment

High density Plasma post-treatment has several purposes. First, changes the structure of carbon nanotubes on their walls and tips. Second, purify of carbon nanotubes by eliminating amorphous carbon. Third, changing the density of CNTs was causing defects on CNTs film. Therefore, to optimize the density of CNTs and obtain better field emission properties, proper plasma post treatments on CNTs are needed.

4.2.1 Mechanism of HDPPT [79]

Etching effects in dry etch system are achieved by either chemical or a physical technique or a combination of chemical/physical techniques, as shown in Fig. 4.6. In a purely chemical effect, the plasma creates reactive species (free reactive radicals) that chemically react with the material on the CNTs surface. Free radicals are electrically neutral species and that have noninert bonding structure. Because of their noninert bonding structure, free radicals are highly reactive. Free single oxygen atom, with six free electrons in its outer orbit instead of eight electrons, would be bonded to other atoms to form the inert electron configurations. It will therefore react quickly with other species to achieve the inert state. The idea in plasma etching is for the reactive neutral species to react with the material to be etched. Volatile by-products of the reaction are removed by the low-pressure pumping system.

To achieve etching with a physical mechanism in Fig. 4.6(a), the plasma provides energetic species (bombarding positive ions) that are accelerated toward the CNTs surface by strong electric fields. The ions physically remove the unprotected CNTs surface material by sputter-etch action. Typically, an inert gas such as argon (Ar) is used. A benefit to this physical etching approach is the strong directionality of the etch, making it possible to achieve highly anisotropic profiles (near vertical sidewalls).

However, a problem is that the species removed by sputtering are not volatile and may redeposit back onto the CNTs surface, causing particulates and chemical contamination.

In most of the models, the ion bombardment enhances one of the steps of the chemical etch process in Fig. 4.6(b), such as surface absorption, etching reaction and formation byproducts, or removal of byproduct or uncreated etchant. For example, the ion bombardment causes damage (breaking bond, etc.) which makes the surface more adapting to chemically react with radicals. In addition, the ion bombardment accelerates the formation of volatile byproducts. The ion bombardment may dislodge or sputtering away etch-byproducts which would otherwise tend to stay on the surface and impede the etch process.

There is a combined physical and chemical mechanism in Fig. 4.6(c) where ionic bombardment improves the chemical etching action. The etch profile is varied from isotropic to anisotropic by adjusting the plasma conditions and gas composition. Combined physical and chemical etching produces are good purification control with fair selectivity and is often preferred for most dry etch processes. Table 4.1 summarizes the different etch parameters for chemical, physical, and combined chemical/physical etching. The advantages from each type depend on the objectives of the each process.

The dry etch system may be designed to operate as either isotropic or anisotropic etching dependent on the direction of the RF electric field relative to the wafer surface. This means that positive ion sputtering can occur on the wafer surface or on the edge of the wafer, respectively. If the field is perpendicular to the wafer surface, then the etching was done by a combination of heavy sputtering positive ions and some chemical reactions of radicals. If the field is parallel the surface on the wafer, very little physical sputtering occurs and the etching is done primarily by chemical reactions between radicals and surface materials. Some basic trends for etching process parameters were

provided in Table 4.2.

4.2.2 Effects of High Density Plasma (HDP) Reaction Ion Etching (RIE) Post Treatment with Argon (Ar) on the Characteristics of CNTs

Figures 4.7-4.10 shows the SEM morphology of CNT PPT under Ar gas on flow rate 10~40sccm and etching time 60 seconds with different ICP (a) as-grown, (b) 250W, (c) 300W ,(d) 400W and (e) 500W. Fig. 4.7(a) shows the average length of CNTs and the diameters of CNTs were 10um and 100um, respectively. They have revealed disordered carbons and other phase particles on the as-grown CNTs surface. Figs. 4.7(b)-(d) show the SEM morphology of the CNTs under ICP power 250W, 300W and 400W. The length and density of CNTs were not changed obviously. This time duration shown that the disordered carbons of the CNTs were etched slightly from the surface of CNTs. Fig. 4.7(e) shows the SEM morphology of the CNTs under ICP power 500W, the length of CNTs and the density of CNTs have been changed. This primary reason is Ar ion bombardment to remove amorphous carbon and any non-alignment CNTs from the surface of CNTs. Fig. 4.8 shows the SEM morphology of the CNTs under Ar 20sccm PPT, the Ar PPT was performed in order to modify structural purification and to vaporize contamination of the CNTs. Ar plasma atoms was physical treatment instead of chemical terminated due to the inertness property of the Ar atoms. Figs. 4.9-4.10 show the SEM morphology after PPT, the CNTs structures were destroyed by the plasma bombardment. This is reason why CNTs structures easily destroyed into other amorphous phases by Ar plasma due to the heavy ions.

Figure 4.11 shows the SEM micrographs of CNTs PPT under Ar 20sccm plasma treatment, ICP power 300W and 60sec etching time with different BIAS power (a) untreated, (b) 50W, (c) 100W, and (d) 150W. The density of the CNTs decreases as BIAS power increasing, which results from the destruction of CNTs during Ar plasma

treatment and more CNTs were significant broken under BIAS power 150W. However, for a larger Bias power condition, the smaller CNTs were significantly reduced and had more highly disordered phases on the CNTs surface. Therefore, BIAS power was expected to generate a very strong Ar atom bombardment to affect the morphology of surface on nanotubes. These new disordered carbons were expected to come from residue carbon particles that were produced by the previous duration of time. The result were revealed that the reduction of CNTs density and induced these new disordered carbons.

Figure 4.8(f) shows Raman spectrum of the CNTs with different PPT conditions. All spectrum clearly display that the peaks at 1350 (D band) and 1580 cm^{-1} (G band). The D band indicates disorder or amorphous carbons, while the G band indicates graphite or ordered carbons in the CNTs. There were no shifts and intensity variation of the peaks after HDPPT. This suggests that the Ar atoms is the inert gas, are not chemically terminated by carbon atoms. The optimum conditions in the Ar PPT are only etching and cleaning process that do not cause any structural changes in the CNTs. Therefore, the Ar plasma can be used as an efficient purification technique of the CNTs without forming any atomic bonding on the CNTs. The disordered phases were not changed obviously on ICP power 250W and 300W. The disordered phases were slightly decreased with ICP power 400W. However, the ID/IG ratio was decreased due to the eliminating amorphous carbons.

The emission characteristics and the corresponding Fowler-Nordheim plots for CNTs with different ICP power from summary results have been shown in Table 4-3. For the conditions of Ar 20sccm and ICP power of 300W, revealed better the field emission properties. The turn-on electrical field of the CNTs field emission diode decreases from 3.1 V/μm to 2.2 V/μm for the untreated CNTs and the plasma

post-treatment CNTs for ICP power of 300W. The emission current density increased from 2.35 to 48 mA/cm^2 with the applied electric field (5 V/μm). The possible reasons of enhanced field emission after PPT is probably due to Ar atoms were physical reaction to remove amorphous carbons. However, the field emissions were poor, as shown in Figs. 4.10-4.11. It is deduced that the production of disordered or other amorphous carbon due to bundle shape phenomena.

The field emission ability of the CNTs was improved by structural enhancement after Ar PPT process, which calculated geometrical enhancement factor **ß** from the corresponding Fowler-Nordheim plots, geometrical enhancement factor **ß** was changed from 1869 to 3463 under Ar 20sccm and the ICP power of 300W.

4.2.3 Effects of High Density Plasma (HDP) Reaction Ion Etching (RIE) Post Treatment of Oxygen (O_2) on the Characteristics of CNTs

Figures. 4.12-4.14 show the SEM micrographs of CNTs PPT under O_2 gas on gas flow rate 5~10 sccm and 60 seconds etching time with different ICP power (a) as-grown, (b) 250W, (c) 300W, (d) 400W and (d) 500W. Figs. 4.12(b) and (c) show a SEM image of the CNTs after PPT, the disordered carbons of the CNTs were etched slightly from the CNT surface. This primary reason was the effects of O_2 oxidation. Figs. 4.12(d) and (e) show the surface of the CNTs was oxidized. Because of each graphite shells in the bamboo-like CNTs is not perfectly parallel to the tube axis, a large number of edges of graphite sheets were exposed to the outermost surface of the CNT. The edges of the CNT must be etched during the oxidation treatment, resulting in a thickness reduction [63]. In addition, this time duration showed an oxidation effect and removal of any other bending CNTs from the CNTs surface, but the density of the CNTs was not clearly changed. Fig. 4.13 shows the SEM morphology under the condition of O_2 10sccm, the O_2 PPT was performed in situ in order to modify the surface structure of CNTs. Due to

oxygen plasma will react with amorphous carbon more easily than with carbon nanotubes so as to the reason why amorphous carbon is eliminated [69]. Oxygen plasma modified the structure of CNTs on the surface, such as reducing the walls of carbon nanotube by way of chemical reaction, produce CO, CO_2 volatility gas and influence density of CNTs. Other reason, the results of SEM analysis shows that the more increase of oxygen amount, the more intensity of carbon decreased gradually. It probably leads to increasing the etching effect on defective structure by affluent O_2 radical and increased the aspect ratio of CNTs, because the thicknesses of CNTs have been reduced by the oxidation-treated [70]. Fig. 4.14 shows the SEM morphology under the condition of O_2 20sccm, O_2 plasma atoms were chemically terminated due to the high free radical atoms to form the production of needle-shape with bundle phenomena or more amorphous carbon from the CNTs surface.

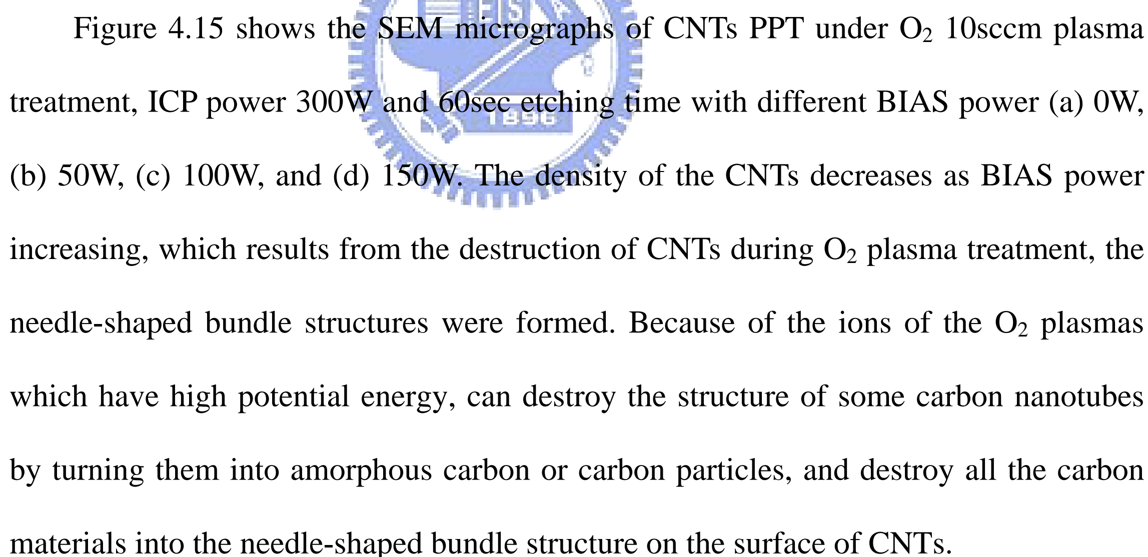

Figure 4.15 shows the SEM micrographs of CNTs PPT under O_2 10sccm plasma treatment, ICP power 300W and 60sec etching time with different BIAS power (a) 0W, (b) 50W, (c) 100W, and (d) 150W. The density of the CNTs decreases as BIAS power increasing, which results from the destruction of CNTs during O_2 plasma treatment, the needle-shaped bundle structures were formed. Because of the ions of the O_2 plasmas which have high potential energy, can destroy the structure of some carbon nanotubes by turning them into amorphous carbon or carbon particles, and destroy all the carbon materials into the needle-shaped bundle structure on the surface of CNTs.

Figure 4.12(f) shows Raman spectrum of the CNTs with different PPT conditions. The ID /IG ratio were decreased due to the eliminating amorphous carbons. However, a large plasma power (O_2 20sccm 500W) increased the ratio of ID/IG due to the production of needle-shape with bundle phenomena or formed more amorphous carbon from the CNTs surface. The O_2 plasma treatment generated oxidation will cause the

changes of CNTs structure. This suggests that O_2 atoms were chemically terminated by carbon atoms because of high reactive radical O_2 atoms.

The emission characteristics and the corresponding Fowler-Nordheim plots for CNTs with different ICP from summary results were shown in Table 4.3. For the condition of O_2 10sccm and ICP power of 300W, revealed better the field emission properties. The turn-on electrical field of the CNTs field emission diode decreases from 3.1 to 2.47 V/μm for the untreated CNTs and the plasma post-treatment CNTs with generated power of 500W. The emission current density at the electric field (5 V/μm) was 2.53 and 12.5 mA/cm^2, respectively, for the untreated CNTs and the CNTs treated under the plasma post-treatment condition of 500W. The field emission ability of the CNTs was improved by structural enhancement after O_2 treatment.

The field emission ability of the CNTs was improved by structural enhancement after Ar PPT treatment., which calculated geometrical enhancement factor **ß** from the corresponding Fowler-Nordheim plots, geometrical enhancement factor **ß** was changed from 1869 to 3130 under O_2 20sccm and the ICP power of 300W.

4.2.4 Effects of High Density Plasma (HDP) Reaction Ion Etching (RIE) Post Treatment of Argon (Ar) and Oxygen (O_2) mixture on the Characteristics of CNTs

Figure 4.15 shows the SEM morphology of CNTs PPT under mixture of Ar and O_2 gas on flow rate 20 and 10 sccm, respectively; the ICP generation power 300W and the 60 seconds etching time with BIAS power : (a) untreated, (b) without BIAS power and (c) with BIAS power. The density of the CNTs decreases as BIAS power increasing, which results from the destruction of CNTs during O_2 plasma treatment, the needle-shaped bundle structures are formed. Because the ions of the plasmas which have high energy, can destroy the structure of some carbon nanotubes by turning them into amorphous carbon or carbon particles, and crush all the carbon materials into the needle-shaped bundle structure on the surface of CNTs. From the SEM image, the CNTs film on the substrate tended to cluster together to form bundles. For the BIAS plasma power, all of CNTs almost were destroyed obviously and it is except that amorphous carbon or carbon particles were existed on the substrate.

The emission characteristics and the corresponding Fowler-Nordheim plots for CNTs with different ICP power from summary results have been shown in Table 4.x. For the conditions of Ar 20sccm and ICP power of 300W, revealed better the field emission properties. The turn-on electrical field of the CNTs field emission diode was increased from 3.1 to 5.08 V/μm for the untreated CNTs and the CNT PPT with BIAS power. The emission current density was decreased from 2.35 to 0.00176 mA/cm^2 at the applied electric field (5 V/μm).

4.3 Fabrication and Characterization of the Carbon Nanotubes Field Emission Triodes with HDPPT

On the selective growth process, carbon nanotubes via the thermal chemical vapor deposition (Thermal CVD) for the low turn-on voltage field emission diodes have been demonstrated successfully. Fig. 4.17(a) show the SEM photograph of the fabricated carbon nanotubes field emission triode, the fabricated device contains 100 x 100 arrays of carbon nanotubes triode field emission cells. It can be seen that carbon nanotubes were selectively grown only on the catalytic Fe-Ni layer but not on the poly silicon gate area of which the aperture is 10 μm in diameter. Furthermore, no inter-connection between gate and carbon nanotubes emitter was observed. Fig. 4.17(b) show the SEM micrograph of the carbon nanotubes inside the emitter area.

Field emission electrical measurement was performed in a high vacuum probing station. The pressure of the system was kept at 10^{-6} Torr during measurement. The DC measurement system is based on Keithley 237 high voltage source units with IEEE488 interface and automatically controlled by computer. The emitter was contacted through the backside of the wafer and a ZnO:Zn phosphor coated ITO glass was applied as the anode, which was positioned about 1 mm above the field emission device surface. No specific treatment was performed before electrical measurement. On the measurement, a constant voltage of 600 V was applied to the anode plate, and the gate voltage swept positively from 0 to 50 V. Figs 4.17(c) and (e) shows the SEM morphology of CNTs and the anode current reaches 1 μA at the gate bias of 50 V under Ar HDPPT. Figs 4.17(d) and (e) shows the SEM morphology of CNTs and the anode current reaches 0.86 μA at the gate bias of 50 V under O_2 HDPPT. A large emission current of 1μA, which equals to an extremely high emission current density of 0.4 mA/cm^2. The triode devices achieved the low turn-on gate voltage of 18 V and the high emission current density of

0.4 mA/cm^2 at 50 V. The results exhibit the carbon nanotubes is the potential application for field emission display.

Chapter 5

Summary and Conclusions

5.1 Synthesis and Properties of CNTs by Thermal CVD

A pre-treatment procedure step causes the catalyst layer to nucleate the nanoparticles which the average size was in proportion to the initial Fe-Ni layer thickness. The catalyst layer with the thickness of 5nm obtained the nanoparticle with the average size of 45nm and the CNTs with the average diameter of 110nm, respectively. The experimental results showed that the diameter of the CNTs was 1.5~2 times as large as the average size of the nano-particle size. Via controlling the density of the CNTs by pre-treatment on the 5nm, the better characteristics of field emission was attained due to the prevention of screening effect and the local field enhancement factor also was enhanced.

A pre-treatment with the CH_4 gas sources can induce the Fe-Ni-C alloy which have a lower Tammann temperature due to the low melting point. The lower Tammnann temperature allows carbon atoms to diffuse fast in Fe-Ni-C catalysts than those in Fe-Ni catalysts. Therefore, the pre-treatment of CH_4 gas can facilitate the formation of CNTs at 500℃.

The addition of N_2 in the process gas not only enhances the nucleation of the CNTs, but also promotes the formation of bamboo-like CNT structures. The role of N_2 for the vertical alignment was due to the N_2 which can keep the catalytic metals active for the nucleation of CNTs. Another possible is conjectured that the N_2 directly suppress the decomposition of C_2H_4 into amorphous carbon. The role of H_2 additions not only cleans the surface of the catalyst layer but also avoids the formation of amorphous carbons.

The well-aligned nanotubes linearly be grown from 5% (10sccm) to 16% (80sccm) for C_2H_4 concentrations, the length of CNTs from 6.8 to 25.3um, respectively. During

the linear growth, the nanotubes grew at a rate of 0.36um/(1min。 10sccm) at 700℃. However, C_2H_4 concentrations above 20%(100sccm), the nanotubes length trended saturation. The reason maybe the catalyst have deactivated in CNTs stop grown or it became more difficult for the reactive carbon species to reach the catalyst particle at the root of the nanotube.

5.2 Effects of Field Emission on the Characteristics of CNTs Diodes HDPPT

The improvement in field emission property of CNTs was also achieved via the density reduction of CNTs and the modification of surface morphology of CNTs by Ar and O_2 high density plasma post treatment (HDPPT). Ar HDPPT exhibited not only physical bombardment (inert atoms) but also purification process. Because of Ar was the inert atom which modified any structural defects and vaporized the contamination on the CNTs. The field emission characteristics therefore are improved under suitable PPT conditions, the field emission current density increased from 2.35 mA/cm^2 to 48 mA/cm^2 at the electric field of 5 V/μm and the turn-on electric field decreased from 3.1 V/μm for the untreated condition to 2.1 V/μm for a HDPPT of a ICP power of 300W, a flow rate of 20sccm, and an etching time of 60sec.

O_2 HDPPT was considered as a chemical etching (free radicals) in order to modify structural defects such as amorphous carbon; etching process will generate a large amount of the defects and change the surface structure of CNTs. A high density of defects cause by the plasma treatment was likely to make the external surface of CNTs more active to emit electrons after treatment. In addition, catalyst particles on the top of the nanotubes can be removed after the plasma treatment. Moreover, the sharp tip of CNTs due to the removal of the catalyst particles may increase the local electrical field more effectively. The field emission characteristics confirmed the improvement of field emission properties under suitable PPT conditions; the field emission current density increased from 2.35 mA/cm^2 to 28 mA/cm^2 at the electric field of 5 V/μm and

the turn-on electric field decreased from 3.1 V/μm for the untreated condition to 2.3 V/μm for a HDPPT one of a generated power of 300W, a O_2 flow rate of 10sccm, and an etching time of 60s. The experimental results reveal that improved emission properties can be achieved by the control of the density and the length of CNTs under proper HDPPT conditions.

The HDPPT with the Ar and O_2 mixture gases reflected not only the physical effect but also the chemical effect. However, the surface of CNT in extreme free active radicals induced needle-shaped bundle result in extra amorphous carbon phase that phenomenon reduced the characteristics of field emission. The field emission characteristics was not improved under HDPPT conditions, the field emission current density decreased from 2.35 mA/cm^2 to 0.17 mA/cm^2 at the electric field of 5 V/μm and the turn-on electric field increased from 3.1 V/μm for the untreated condition to 4.5 V/μm for the PPT one of a ICP power of 300W, an Ar flow rate of 20sccm, an O_2 flow rate of 10sccm, and an etching time of 60s.

Based on the diode HDPPT conditions, further reduced the operation voltage of the field emission triodes with CNTs. The trench-type CNT triodes have been successfully fabricated using the oxide as the gate insulator. The spacing between the gate and the emitter fixed at 150um to prevent CNTs short problem. The turn-on voltages were 18V for the CNT lengths of 5um after HDPPT. Correspondingly, the anode current 1uA can be achieved at the gate voltage of 50V. These excellent properties offer the promising application of the CNT field emission triodes for the vacuum microelectronics and flat panel displays.